

Enhancing strontium clock atom interferometry using quantum optimal control

Zilin Chen, Garrett Louie, Yiping Wang, Tejas Deshpande, Tim Kovachy

Department of Physics and Astronomy and Center for Fundamental Physics, Northwestern University

Strontium clock atom interferometry is a promising new technique, with multiple experiments under development to explore its potential for dark matter and gravitational wave detection. In these detectors, large momentum transfer (LMT) using sequences of many laser pulses is necessary, and thus high fidelity of each pulse is important since small infidelities become magnified. Quantum Optimal Control (QOC) is a framework for developing control pulse waveforms that achieve high fidelity and are robust against experimental imperfections. Resonant single-photon transitions using the narrow clock transition of strontium involve significantly different quantum dynamics than more established atom interferometry methods based on far-detuned two-photon Raman or Bragg transitions, which leads to new opportunities and challenges when applying QOC. Here, we study QOC pulses for strontium clock interferometry and demonstrate their advantage over basic square pulses (primitive pulses) and composite pulses in terms of robustness against multiple noise channels. This could improve the scale of large momentum transfer in Sr clock interferometers, paving the way to achieve these scientific goals.

Light-pulse atom interferometry has proven itself a powerful tool for precision metrology and sensing, with applications including tests of quantum mechanics and the equivalence principle [1–15], terrestrial and space-borne gravitational wave detection [16–25], precision measurements of the fine structure constant [26–28] and gravity [29, 30], searches for dark matter [31, 32] and dark energy [33], and mobile surveying [34, 35]. The most sensitive interferometers employ large momentum transfer (LMT) techniques, which increase the enclosed spacetime area with additional laser pulses. Typical LMT atom optics utilize far detuned, multi-photon transitions [36–46], where two ground states are coupled via a short-lived excited state. The scaling of such pulse sequences is limited by spontaneous emission, which can only be mitigated so long as additional laser power is available.

In contrast, alkaline earth atoms such as Sr possess long lived excited states, which have been leveraged to achieve the state of the art atomic clocks [47, 48]. In ^{87}Sr , the $^1\text{S}_0 \rightarrow ^3\text{P}_0$ clock transition has a lifetime in excess of 100 seconds, allowing resonant, single-photon atom optics with greatly reduced spontaneous emission losses. This affords an enormous increase in available pulse area, potentially scalable to thousands of pulses before spontaneous emission losses become significant [25, 49]. Clock interferometry also offers improved laser phase noise rejection in differential measurement configurations comparing multiple interferometers over a long baseline [18] [50], which is essential for dark matter and gravitational wave detection. Moreover, the clock transitions in alkaline earth atoms are orders of magnitude less susceptible to magnetic fields than in the alkalis [51]. This new generation of recently demonstrated single-photon clock atom interferometers [49, 52–54] is poised to study hitherto elusive phenomena such as ultralight, wavelike dark matter [22, 23, 25, 31, 32], tests of atom charge neutrality [55], mid-band gravitational wave detection [22, 23, 25], and tests of quantum mechanics at unprecedented delocalization scales [25].

In practice, the performance of atom interferometers

is also limited by noise in the driving field and inhomogeneities across the atom cloud. Atom losses and phase errors caused by these effects accumulate with repeated pulses and thus limit the scaling of LMT systems. Simple robust control pulses for two level quantum systems under detuning and amplitude errors were developed for nuclear magnetic resonance (NMR) spectroscopy [56, 57] and have more recently found popularity in quantum computation [58–60]. More sophisticated pulse shaping algorithms, such as gradient ascent pulse engineering (GRAPE) [61] and chopped random basis (CRAB) optimization [62, 63], minimize a cost function which quantifies the infidelity of the operation. As this may be an arbitrary function of hundreds of parameters, highly modulated control pulses can now be tailor made for driving particular quantum dynamics with an appropriate cost metric. For instance, quantum optimal control is a powerful tool for realizing high-fidelity gates in quantum computing [64–66].

In the field of atom interferometry, quantum control schemes including composite pulses [67, 68], shaped pulses [57, 69], adiabatic rapid passage [44, 70], and numerical optimal control [71–74] have been applied to Raman and Bragg transitions with alkalis. In this paper, we report simulation studies of numerical optimal control's applications to clock interferometry with ^{87}Sr . Using the gradient based optimization tools in Q-CTRL's BOULDER OPAL package [75], we design optimized analogues of π pulses which are robust to as many as five simultaneous noise channels. Sequences of many of these pulses can be used to achieve enhanced LMT [17]. Under an experimentally relevant range of noise, we find that the optimized pulses have fidelity improved beyond that of basic square (primitive) pulses by an order of magnitude or more. Successful implementation of these pulses may allow atom interferometers to overcome unavoidable limitations and realize their full potential.

A new challenge in clock interferometry is the importance of the laser's polarization. Imperfections during laser beam delivery or local changes to the quantization

axis from stray magnetic fields can introduce undesired polarization components, which couple transitions to additional magnetic sublevels (Fig. 1a). Larger bias fields can suppress errors in the quantization axis, but are unfavorable due to quadratic Zeeman shifts [25] and unable to mitigate errors already present in the beam. It is therefore a practical application of quantum optimal control to design pulses which are insensitive to polarization defects and thus reduce the atom loss and phase errors arising from the population of other sublevels.

In the interferometry scheme studied here—which is applicable, for instance, to clock-transition-based dark matter and gravitational wave detectors [18, 31]—a cloud of ^{87}Sr atoms is initialized in the $|^1\text{S}_0; m_F = 9/2\rangle$ state and driven to the $|^3\text{P}_0; m = 9/2\rangle$ state on the 698 nm clock transition, which has a natural linewidth of 1 mHz [25]. For optimization, we split a pulse of fixed duration uniformly into N time segments, whose amplitude and phase become the $2N$ independent variables, hereafter referred to as \mathbf{c} , which are modified during optimization. The pulse duration and the number of segments are chosen before optimization, as is the learning rate (the step size in the gradient-based search). We manually vary these parameters between optimization runs to determine what gives the best results. We choose maximum Rabi frequencies of several kHz [25] and find pulse lengths of 2 ms or longer best for optimizing against all noise channels. With the many-second interferometer durations in tall atomic fountains [25] or spaceborne detectors [16, 21, 22], sequences of thousands of pulses may be performed, further increased by future upgrades to laser power [76, 77]. In the optimized pulse, the segment time is approximately $17\ \mu\text{s}$, which is significantly longer than an acousto-optic modulator (AOM) response time.

To achieve robust control, we design a cost function based on random sampling of noise trajectories. We include five channels of static noise: σ_+ and σ_- polarization components, which couple sublevels outside the desired two level system; amplitude noise on the drive; detuning errors from Doppler shifts in the atom cloud; and variation in the bias field, which changes the Zeeman splitting of the sublevels. Each channel is associated with a Hamiltonian term \hat{N}_j . For each of these operators, we randomly sample n_B noise amplitudes—which we denote as $\boldsymbol{\beta}^{(i)} = (\beta_1^{(i)}, \beta_2^{(i)}, \dots, \beta_5^{(i)})$ for the i th noise trajectory in the batch—from Gaussian distributions whose predefined width determines the scope of desired robustness. The Hamiltonian for the i th trajectory is thus

$$\hat{H}^{(i)}(\mathbf{c}, t) = \hat{H}_0 + \hat{H}_c(\mathbf{c}, t) + \hat{\mathbf{N}} \cdot \boldsymbol{\beta}^{(i)}(t) \quad (1)$$

where \hat{H}_0 describes the free evolution of the system, and \hat{H}_c is the control term from the driving pulse. $\beta_j^{(i)}$ are not time dependent except for the amplitude noise, which remains proportional to the control by a constant factor for the duration of the pulse. For each of these n_B Hamiltonians, we calculate the unitary evolution, from which we determine an infidelity $\mathcal{I}^{(i)}(\mathbf{c})$. All 20 ground and excited

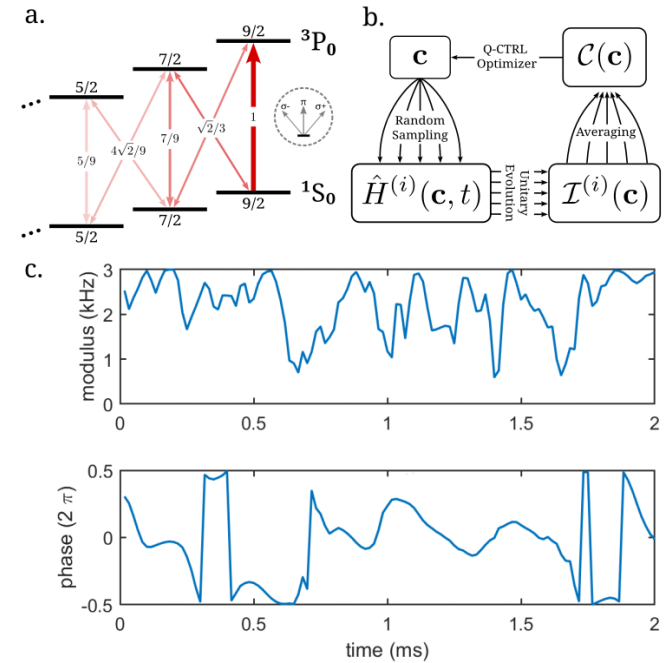


FIG. 1. (a) Substructure of the $^1\text{S}_0$ and $^3\text{P}_0$ manifolds, with transition strengths indicated. Parasitic σ_+ and σ_- polarizations couple to states outside the desired $m = 9/2 \rightarrow m' = 9/2$ two-level system. (b) Optimization procedure. Randomly sampled noise values for multiple noise channels define a batch of noise trajectories. The unitary evolution of the system is calculated under each, yielding a batch of infidelities which are averaged to give the final cost function. The scope of robustness is tuned by modifying the sampling distributions. (c) Optimized pulse, showing phase and amplitude modulation smoothed with a Gaussian-weighted moving average filter.

sublevels are included in our simulations. To construct the total cost function, we average the infidelities from all trajectories:

$$\mathcal{C}(\mathbf{c}) = \frac{1}{n_B} \sum_{i=1}^{n_B} \mathcal{I}^{(i)}(\mathbf{c}) \quad (2)$$

We typically use an n_{batch} of around 200. The gradient-based optimizer in BOULDER OPAL determines the control variables \mathbf{c} which minimize this cost function. Thus, pulse waveforms are determined which retain low infidelity even in the presence of noise.

We primarily use an infidelity defined as

$$\mathcal{I}^{(i)}(\mathbf{c}) = 1 - \left| \frac{\text{Tr} \left(U_{\text{target}}^\dagger U^{(i)}(\mathbf{c}) \right)}{\text{Tr} \left(U_{\text{target}}^\dagger U_{\text{target}} \right)} \right|^2 \quad (3)$$

where U_{target} is the target operation, and $U^{(i)}$ is the operation due to the Hamiltonian under the i th noise trajectory [75]. This metric is sensitive to both the population transfer and the phase imprinted by the pulse, which is important for atom interferometry.

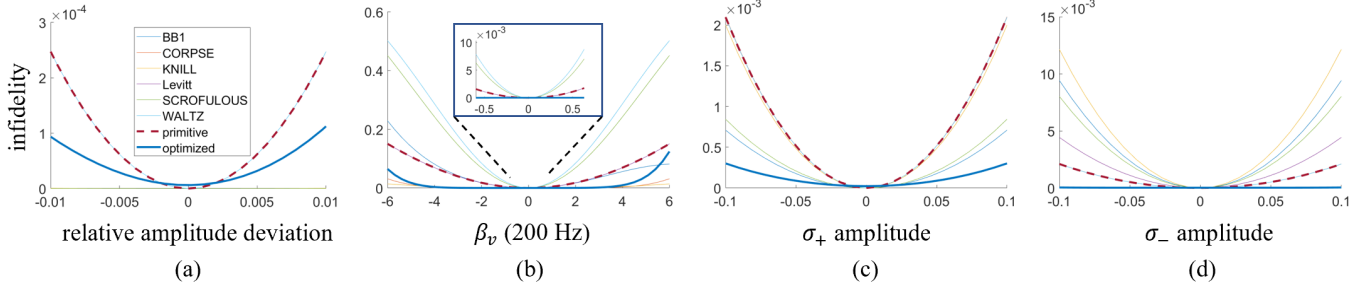


FIG. 2. Comparison of optimized pulse to primitive pulse and various composite pulses [56, 71]. Single pulse infidelity with noise parameters' variation are compared among the optimized pulse, primitive pulse, and composite pulses. In contrast to all other pulses, the optimized pulse maintains a high degree of robustness against all noise channels, and the optimized pulse outperforms all other pulses in robustness against polarization noise. In (a), SCROFULOUS, KNILL and BB1 composite pulses outperform the optimized pulse in robustness against pulse amplitude noise (these curves are close to 0). The curves corresponding to Levitt, CORPSE, and WALTZ composite pulses overlap with the primitive pulse curve, and these pulses perform worse than the optimized pulse. In (b), the parameter β_v represents pulse detuning (which can be caused by Doppler shifts), in units of 200 Hz (for comparison, the peak Rabi frequency is 3 kHz). (c) and (d) show infidelity vs. relative polarization amplitude in σ_+ and σ_- components, respectively. In (c), WALTZ, Levitt, CORPSE, and KNILL curves overlap with the primitive pulse curve. In (d), CORPSE and WALTZ curves overlap with the primitive pulse curve.

To visualize the performance of various pulse schemes, we scan the infidelity across values of one (Fig. 2) or two (Fig. 3) noise channels. The range of noise values in optimization and in these plots follows what is expected in relevant experiments. In dark matter and gravitational wave experiments, it is favorable for the atom cloud's spatial extent to remain within the central region of the laser beam to help mitigate systematic errors such as those due to laser wavefront perturbations and residual AC Stark shifts from far-detuned transitions [25]. Therefore the laser amplitude variation across the atom cloud is assumed to be within $\pm 1\%$. We also assume Doppler shifts to be on the order of 500 Hz, which is consistent with atom clouds lensed to sub-nK effective temperatures [25, 78] that are desirable for systematic error mitigation in dark matter and gravitational wave detectors [25]. A 0.1 polarization amplitude error gives a reasonable 1% of optical power in unwanted components. In general, the amplitudes of the σ_+ and σ_- polarization components can be complex. While Fig. 2 plots values of these amplitudes over a real domain to ease visualization, we note that using complex values for these coefficients does not significantly affect the size of the infidelities. Variations in the bias magnetic field generally have a smaller impact on the infidelity compared with other noise channels.

As shown in Fig. 2, the optimized pulse performs up to an order of magnitude better than the composite pulses for the range of polarization errors considered here while maintaining strong robustness against amplitude and detuning errors. The control pulse that we evaluate is optimized based on a simple cost function (infidelity) which accounts for both phase deviation and transfer efficiency in a particular way (see Eqn. 3). In some applications, it may be useful to adjust the relative weightings on the phase deviation using other cost functions.

Another series of cost function candidates are p -norms,

with the p th order norm defined as

$$C_p(\mathbf{c}) = \sqrt[p]{\frac{1}{n_B} \sum_i^{n_B} \left| 1 - \text{Im} \langle \psi_{\text{target}} | U^{(i)}(\mathbf{c}) | \psi_0 \rangle \right|^p} \quad (4)$$

where $|\psi_{\text{target}}\rangle = |^3\text{P}_0; m = 9/2\rangle$ is the intended final state and $|\psi_0\rangle = |^1\text{S}_0; m_F = 9/2\rangle$ is the initial state. We test adding these terms to cost functions calculated from Eqn. 3, as well as optimizing for the p -norms alone.

Fig. 3 shows fidelities and phase deviations as functions of polarization errors from optimized pulses using cost functions respectively based on infidelity, the sum of infidelity and the first order norm, and the first order norm alone. Phase deviations arising from other noise channels in the ranges indicated in Fig. 2 are of a comparable scale. The alternative cost functions reduce phase deviations by a factor of approximately three while only modestly affecting the robustness of the fidelity, making these cost functions potentially useful choices. Nevertheless, the original optimization using infidelity for the cost function may remain a suitable choice for many applications due to the relatively small phase error from each pulse. For the \sim mrad phase deviations associated with the polarization error ranges shown in Fig. 3, an atom interferometer with ~ 1000 pulses would introduce a total \sim rad scale phase deviation. Atomic dark matter and gravitational wave detectors typically look for time varying signals in a particular frequency band, such as 0.3 - 3 Hz [25]. If, for example, the fractional fluctuation of the polarization errors are at the level of $0.1\%/\sqrt{\text{Hz}}$ in this frequency band, the corresponding interferometer phase noise would be at the level of \sim mrad/ $\sqrt{\text{Hz}}$. Such phase fluctuations may be further suppressed if both arms of the interferometer, or both interferometers in a differential gradiometer configuration [25], experience close to

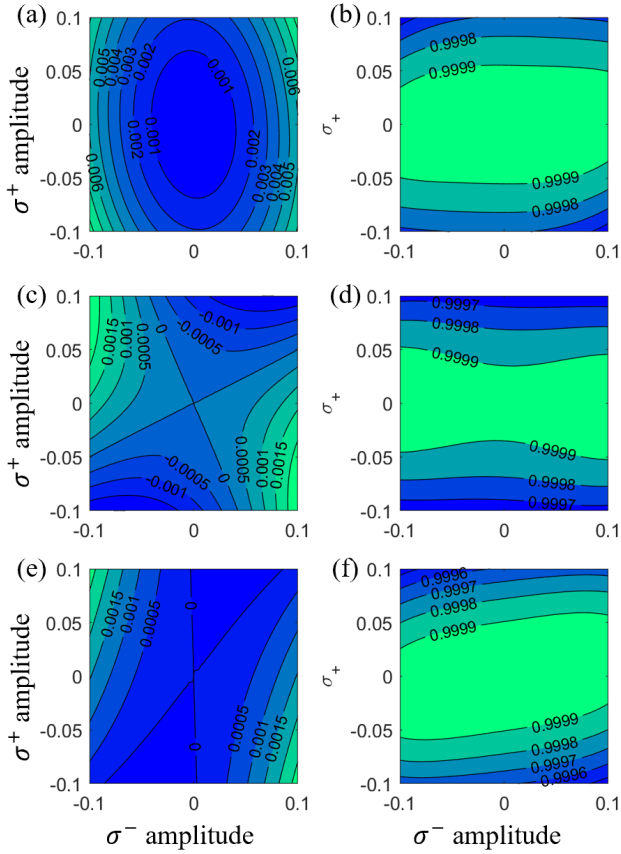


FIG. 3. Comparison among different cost functions used in the optimization. (a), (c), (e) respectively show the phase deviation (in rad) of optimizations using infidelity, the sum of infidelity with 1-norm, and only 1-norm as cost function. Using 1-norm in the cost function in the optimization reduces phase deviation by a factor of approximately 3, while the robustness of infidelity against noise channels such as polarization errors [(b), (d), (f)] gets minor impacts.

the same polarization errors.

Since time dependent noise in the laser amplitude and phase will also occur in the physical system, we studied its impact on the robustness of the optimized pulse. The added noise is constructed by

$$f(t) = \sum_i^{20} A_i \cos(\omega_i t) + B_i \sin(\omega_i t), \quad (5)$$

where A_i and B_i are randomly generated amplitudes and ω_i are random frequencies uniformly distributed from 50 Hz to 10^5 Hz. To control the RMS of the generated noise, we normalize each $f(t)$ so that it has the desired RMS value. The spectrum of the noise is chosen in this range since lower or higher frequencies are tested to have less impact on the robustness of the control pulse. Since the noise is randomly generated for each simulation, the impact on infidelity undergoes some fluctuation between different simulation runs. We measure this impact by plotting the trend of the area in the contour plot whose

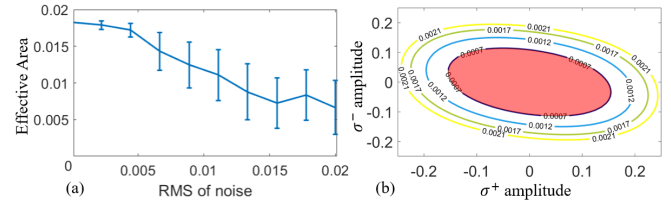


FIG. 4. Noise impact on infidelities. In (a), for the same optimized pulse, adding noises in the control pulse will negatively impact the robustness. The way we measure the noise impact on the performance is to measure effective area (red) where the infidelity is under 0.0007 in the polarization map in (b). With the root mean square (RMS) of the noise increasing, the effective area decreases. Due to the randomness of the noise generator, the impact of the noise varies in every simulation, thus the standard deviation from repeated simulations is used as error bars in (a). A value x of the RMS of noise on the horizontal axis of the plot corresponds to RMS fractional amplitude noise of x and RMS phase noise of x rad.

infidelity is under a certain value (effective area). By repeating the simulations, the impact fluctuations are indicated by error bars (standard deviation), and the trend is shown in Fig. 4(a). Overall, with bigger noise both in amplitude and phase, the effective area is smaller in the polarization map, and a similar scale of area reduction is observed for other parameters. For the noise magnitudes considered here, the effective area reduction is relatively modest (a factor of approximately 2 or less), indicating that the optimized pulses can remain effective in the presence of noise.

In the atom interferometers considered here, an initial $\pi/2$ pulse splits the atom into a superposition of two trajectories with different momenta which form the two interferometer arms. Then, sequences of π pulses (or optimized pulses filling the role of π pulses) with the laser frequency adjusted to remain resonant with one arm continue to transfer additional momentum to that arm (transferred arm), increasing the momentum splitting between the arms [17]. However, these pulses can also affect the other arm (untransferred arm). In Fig. 5(a), (b)], the population in the untransferred arm remaining in the desired state (i.e., not undergoing unwanted transfer to another state) is shown. The effect on the untransferred atoms can be made small by using primitive pulses with appropriate Rabi frequency, and thus most atoms in the untransferred arm can stay in the interferometer (5(a)). On the other hand, when the relative Doppler shift between the two arms is small for the initial momentum splitting pulses, the optimized pulse strongly affects the untransferred arm. As the relative velocity between the arms increases, the increasing relative Doppler shift causes the pulses to become further detuned from the untransferred arm, and the effect of the optimized pulses on the untransferred arm decreases. To avoid the deleterious effects of the optimized pulse on the untransferred arm at small momentum separations,

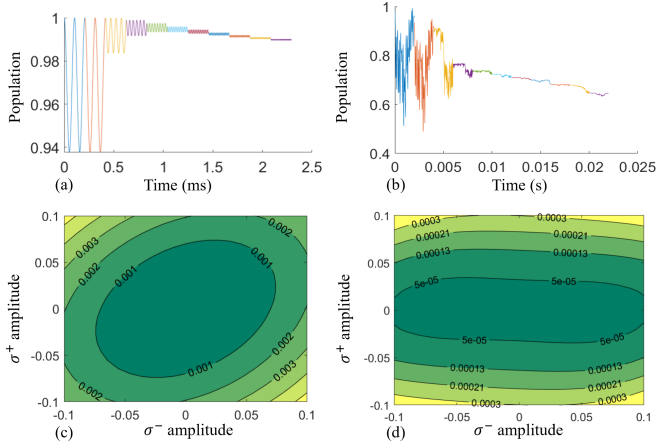


FIG. 5. In (a) and (b), the population remaining in the untransferred arm during an initial sequence of 11 momentum splitting pulses (different colors represent different pulses) is shown for a primitive [(a)] and optimized [(b)] pulse, respectively. The primitive pulse can affect the untransferred arm for these initial pulses where the Doppler detuning between the two arms is small, but by adjusting the Rabi frequency effect can be minimized as shown in (a). In (b), the optimized pulses have a strong effect on the untransferred arm for small Doppler detunings. Therefore, using primitive pulses for the initial momentum splitting and optimized pulses to enhance the momentum splitting once a larger Doppler shift has accumulated is a practical option. (c) and (d) show infidelity maps (over polarization) of a single primitive pulse and optimized pulse, respectively, for the transferred arm, demonstrating the superior performance of the optimized pulse.

a preferable approach is using primitive pulses for the initial $\pi/2$ pulse and for an initial small amount of momentum transfer so that infidelities remain small, and then using the optimized pulse to boost the momentum splitting to large values (for example, primitive pulses for the initial 50 splitting pulses out of 1000 pulses in total).

In summary, this work demonstrates the promise of quantum optimal control for extending the scientific reach of strontium clock atom interferometers, potentially paving the way for these interferometers to detect gravitational waves at currently unexplored frequencies and wavelike dark matter. Future work will study the experimental implementation of the optimized pulses. To achieve best performance, it may prove valuable to tailor the noise model used in the optimization algorithm to specific, experimentally measured noise spectra. The application of closed-loop quantum optimal control [79], in which experimental measurements of pulse fidelities guide the optimization process, to atom interferometry has the potential to offer further improvements.

ACKNOWLEDGMENTS

We thank Jens Koch, Yunwei Lu, and Q-CTRL for valuable discussions. This material is based upon work supported by the U.S. Department of Energy, Office of Science, National Quantum Information Science Research Centers, Superconducting Quantum Materials and Systems Center (SQMS) under contract number DE-AC02-07CH11359.

[1] L. Zhou, S. Long, B. Tang, X. Chen, F. Gao, W. Peng, W. Duan, J. Zhong, Z. Xiong, J. Wang, Y. Zhang, and M. Zhan, Phys. Rev. Lett. **115**, 013004 (2015).

[2] G. Rosi, G. D'Amico, L. Cacciapuoti, F. Sorrentino, M. Prevedelli, M. Zych, Č. Brukner, and G. Tino, Nat. Comm. **8**, 1 (2017).

[3] C. Overstreet, P. Asenbaum, T. Kovachy, R. Notermans, J. M. Hogan, and M. A. Kasevich, Phys. Rev. Lett. **120**, 183604 (2018).

[4] P. Asenbaum, C. Overstreet, M. Kim, J. Curti, and M. A. Kasevich, Phys. Rev. Lett. **125**, 191101 (2020).

[5] T. Kovachy, P. Asenbaum, C. Overstreet, C. Donnelly, S. Dickerson, A. Sugarbaker, J. Hogan, and M. Kasevich, Nature **528**, 530 (2015).

[6] S. Fray, C. A. Diez, T. W. Hänsch, and M. Weitz, Phys. Rev. Lett. **93**, 240404 (2004).

[7] D. Schlippert, J. Hartwig, H. Albers, L. L. Richardson, C. Schubert, A. Roura, W. P. Schleich, W. Ertmer, and E. M. Rasel, Phys. Rev. Lett. **112**, 203002 (2014).

[8] B. Barrett, L. Antoni-Micollier, L. Chichet, B. Battelier, T. Lévèque, A. Landragin, and P. Bouyer, Nat. Comm. **7**, 13786 (2016).

[9] C. C. N. Kuhn, G. D. McDonald, K. S. Hardman, S. Bennetts, P. J. Everitt, P. A. Altin, J. E. Debs, J. D. Close, and N. P. Robins, New J. Phys. **16**, 073035 (2014).

[10] B. Barrett, L. Antoni-Micollier, L. Chichet, B. Battelier, P.-A. Gominet, A. Bertoldi, P. Bouyer, and A. Landragin, New J. Phys. **17**, 085010 (2015).

[11] M. G. Tarallo, T. Mazzoni, N. Poli, D. V. Sutyrin, X. Zhang, and G. M. Tino, Phys. Rev. Lett. **113**, 023005 (2014).

[12] A. Bonnin, N. Zahzam, Y. Bidel, and A. Bresson, Phys. Rev. A **88**, 043615 (2013).

[13] J. Hartwig, S. Abend, C. Schubert, D. Schlippert, H. Ahlers, K. Posso-Trujillo, N. Gaaloul, W. Ertmer, and E. M. Rasel, New J. Phys. **17**, 035011 (2015).

[14] J. Williams, S. Wey Chiow, N. Yu, and H. Müller, New J. Phys. **18**, 025018 (2016).

[15] C. Overstreet, P. Asenbaum, J. Curti, M. Kim, and M. A. Kasevich, Science **375**, 226 (2022).

[16] S. Dimopoulos, P. W. Graham, J. M. Hogan, M. A. Kasevich, and S. Rajendran, Phys. Rev. D **78**, 122002 (2008).

[17] P. W. Graham, J. M. Hogan, M. A. Kasevich, and S. Rajendran, Phys. Rev. Lett. **110**, 171102 (2013).

[18] P. W. Graham, J. M. Hogan, M. A. Kasevich, and S. Rajendran, Phys. Rev. D **94**, 104022 (2016).

[19] W. Chaibi, R. Geiger, B. Canuel, A. Bertoldi, A. Landragin, and P. Bouyer, Phys. Rev. D **93**, 021101 (2016).

[20] B. Canuel, A. Bertoldi, L. Amand, E. Pozzo di Borgo, T. Chantrait, C. Danquigny, M. Dovale Álvarez, B. Fang, A. Freise, R. Geiger, *et al.*, *Sci. Rep.* **8**, 1 (2018).

[21] J. M. Hogan, D. Johnson, S. Dickerson, T. Kovachy, A. Sugarbaker, S.-w. Chiow, P. W. Graham, M. A. Kasevich, B. Saif, S. Rajendran, *et al.*, *Gen. Relativ. Gravit.* **43**, 1953 (2011).

[22] Y. A. El-Neaj, C. Alpignani, S. Amairi-Pyka, H. Araújo, A. Balaž, A. Bassi, L. Bathe-Peters, B. Battelier, A. Belić, E. Bentine, J. Bernabeu, A. Bertoldi, R. Birmingham, *et al.*, *EPJ Quantum Technol.* **7**, 6 (2020).

[23] L. Badurina, E. Bentine, D. Blas, K. Bongs, D. Bortolotto, T. Bowcock, K. Bridges, W. Bowden, O. Buchmueller, C. Burrage, J. Coleman, G. Elertas, J. Ellis, C. Foot, V. Gibson, M. Haehnelt, T. Harte, S. Hedges, R. Hobson, M. Holynski, T. Jones, M. Langlois, S. Lelouch, M. Lewicki, R. Maiolino, P. Majewski, S. Malik, J. March-Russell, C. McCabe, D. Newbold, B. Sauer, U. Schneider, I. Shipsey, Y. Singh, M. Uchida, T. Valenzuela, M. van der Grinten, V. Vaskonen, J. Vossebeld, D. Weatherill, and I. Wilmut, *J. Cosmol. Astropart. Phys.* **2020** (05), 011.

[24] M.-S. Zhan, J. Wang, W.-T. Ni, D.-F. Gao, G. Wang, L.-X. He, R.-B. Li, L. Zhou, X. Chen, J.-Q. Zhong, B. Tang, Z.-W. Yao, L. Zhu, Z.-Y. Xiong, S.-B. Lu, G.-H. Yu, Q.-F. Cheng, M. Liu, Y.-R. Liang, P. Xu, X.-D. He, M. Ke, Z. Tan, and J. Luo, *Int. J. Mod. Phys. D* **29**, 1940005 (2020).

[25] M. Abe, P. Adamson, M. Borcean, D. Bortolotto, K. Bridges, S. P. Carman, S. Chattopadhyay, J. Coleman, N. M. Curfman, K. DeRose, *et al.*, *Quantum Sci. Technol.* **6**, 044003 (2021).

[26] R. Bouchendira, P. Cladé, S. Guellati-Khélifa, F. m. c. Nez, and F. m. c. Biraben, *Phys. Rev. Lett.* **106**, 080801 (2011).

[27] R. H. Parker, C. Yu, W. Zhong, B. Estey, and H. Müller, *Science* **360**, 191 (2018).

[28] L. Morel, Z. Yao, P. Cladé, and S. Guellati-Khélifa, *Nature* **588**, 61 (2020).

[29] G. W. Biedermann, X. Wu, L. Deslauriers, S. Roy, C. Mahareshwaraswamy, and M. A. Kasevich, *Phys. Rev. A* **91**, 033629 (2015).

[30] G. Rosi, F. Sorrentino, L. Cacciapuoti, M. Prevedelli, and G. Tino, *Nature* **510**, 518 (2014).

[31] A. Arvanitaki, P. W. Graham, J. M. Hogan, S. Rajendran, and K. Van Tilburg, *Phys. Rev. D* **97**, 075020 (2018).

[32] P. W. Graham, D. E. Kaplan, J. Mardon, S. Rajendran, and W. A. Terrano, *Phys. Rev. D* **93**, 075029 (2016).

[33] P. Hamilton, M. Jaffe, P. Haslinger, Q. Simmons, H. Müller, and J. Khoury, *Science* **349**, 849 (2015).

[34] X. Wu, Z. Pagel, B. S. Malek, T. H. Nguyen, F. Zi, D. S. Scheirer, and H. Müller, *Sci. Adv.* **5**, eaax0800 (2019), <https://www.science.org/doi/pdf/10.1126/sciadv.aax0800>.

[35] K. Bongs, M. Holynski, J. Vovrosh, P. Bouyer, G. Condon, E. Rasel, C. Schubert, W. P. Schleich, and A. Roura, *Nat. Rev. Phys.* **1**, 731 (2019).

[36] J. M. McGuirk, M. J. Snadden, and M. A. Kasevich, *Phys. Rev. Lett.* **85**, 4498 (2000).

[37] H. Müller, S.-w. Chiow, Q. Long, S. Herrmann, and S. Chu, *Phys. Rev. Lett.* **100**, 180405 (2008).

[38] H. Müller, S.-w. Chiow, S. Herrmann, and S. Chu, *Phys. Rev. Lett.* **102**, 240403 (2009).

[39] P. Cladé, S. Guellati-Khélifa, F. m. c. Nez, and F. m. c. Biraben, *Phys. Rev. Lett.* **102**, 240402 (2009).

[40] M. Gebbe, J.-N. Siemß, M. Gersemann, H. Müntinga, S. Herrmann, C. Lämmerzahl, H. Ahlers, N. Gaaloul, C. Schubert, K. Hammerer, *et al.*, *Nat. Comm.* **12**, 1 (2021).

[41] S.-w. Chiow, T. Kovachy, H.-C. Chien, and M. A. Kasevich, *Phys. Rev. Lett.* **107**, 130403 (2011).

[42] G. D. McDonald, C. C. N. Kuhn, S. Bennetts, J. E. Debs, K. S. Hardman, M. Johnsson, J. D. Close, and N. P. Robins, *Phys. Rev. A* **88**, 053620 (2013).

[43] T. Mazzoni, X. Zhang, R. Del Aguila, L. Salvi, N. Poli, and G. M. Tino, *Phys. Rev. A* **92**, 053619 (2015).

[44] K. Kotru, D. L. Butts, J. M. Kinast, and R. E. Stoner, *Phys. Rev. Lett.* **115**, 103001 (2015).

[45] B. Plotkin-Swing, D. Gochnauer, K. E. McAlpine, E. S. Cooper, A. O. Jamison, and S. Gupta, *Phys. Rev. Lett.* **121**, 133201 (2018).

[46] Z. Pagel, W. Zhong, R. H. Parker, C. T. Olund, N. Y. Yao, and H. Müller, *Phys. Rev. A* **102**, 053312 (2020).

[47] N. Hinkley, J. A. Sherman, N. B. Phillips, M. Schioppo, N. D. Lemke, K. Belyov, M. Pizzocaro, C. W. Oates, and A. D. Ludlow, *Science* **341**, 1215 (2013).

[48] B. Bloom, T. Nicholson, J. Williams, S. Campbell, M. Bishop, X. Zhang, W. Zhang, S. Bromley, and J. Ye, *Nature* **506**, 71 (2014).

[49] J. Rudolph, T. Wilkason, M. Nantel, H. Swan, C. M. Holland, Y. Jiang, B. E. Garber, S. P. Carman, and J. M. Hogan, *Phys. Rev. Lett.* **124**, 083604 (2020).

[50] For atom interferometers based on two-photon atom optics, multiple baselines can be used to achieve improved laser noise suppression [20].

[51] A. V. Taichenachev, V. I. Yudin, C. W. Oates, C. W. Hoyt, Z. W. Barber, and L. Hollberg, *Phys. Rev. Lett.* **96**, 083001 (2006).

[52] L. Hu, N. Poli, L. Salvi, and G. M. Tino, *Phys. Rev. Lett.* **119**, 263601 (2017).

[53] L. Hu, E. Wang, L. Salvi, J. N. Tinsley, G. M. Tino, and N. Poli, *Classical Quantum Gravity* **37**, 014001 (2019).

[54] T. Wilkason, M. Nantel, J. Rudolph, Y. Jiang, B. E. Garber, H. Swan, S. P. Carman, M. Abe, and J. M. Hogan, arXiv preprint arXiv:2205.06965 (2022).

[55] A. Arvanitaki, S. Dimopoulos, A. A. Geraci, J. Hogan, and M. Kasevich, *Phys. Rev. Lett.* **100**, 120407 (2008).

[56] M. H. Levitt, *Progress in Nuclear Magnetic Resonance Spectroscopy* **18**, 61 (1986).

[57] L. Emsley and G. Bodenhausen, *J Magn. Reson.* **97**, 135 (1992).

[58] H. K. Cummins, G. Llewellyn, and J. A. Jones, *Phys. Rev. A* **67**, 042308 (2003).

[59] E. Collin, G. Ithier, A. Aassime, P. Joyez, D. Vion, and D. Esteve, *Phys. Rev. Lett.* **93**, 157005 (2004).

[60] L. M. K. Vandersypen and I. L. Chuang, *Rev. Mod. Phys.* **76**, 1037 (2005).

[61] N. Khaneja, T. Reiss, C. Kehlet, T. Schulte-Herbrüggen, and S. J. Glaser, *J Magn. Reson.* **172**, 296 (2005).

[62] P. Doria, T. Calarco, and S. Montangero, *Phys. Rev. Lett.* **106**, 190501 (2011).

[63] T. Caneva, T. Calarco, and S. Montangero, *Phys. Rev. A* **84**, 022326 (2011).

[64] M. Grace, C. Brif, H. Rabitz, I. A. Walmsley, R. L. Kosut, and D. A. Lidar, *J Phys. B* **40**, S103 (2007).

[65] P. Rebentrost, I. Serban, T. Schulte-Herbrüggen, and F. K. Wilhelm, *Phys. Rev. Lett.* **102**, 090401 (2009).

[66] M. Abdelhafez, B. Baker, A. Gyenis, P. Mundada, A. A. Houck, D. Schuster, and J. Koch, *Phys. Rev. A* **101**, 022321 (2020).

[67] A. Dunning, R. Gregory, J. Bateman, N. Cooper, M. Himsworth, J. A. Jones, and T. Freegarde, *Phys. Rev. A* **90**, 033608 (2014).

[68] P. Berg, S. Abend, G. Tackmann, C. Schubert, E. Giese, W. P. Schleich, F. A. Narducci, W. Ertmer, and E. M. Rasel, *Phys. Rev. Lett.* **114**, 063002 (2015).

[69] Y. Luo, S. Yan, Q. Hu, A. Jia, C. Wei, and J. Yang, *Eur. Phys. J. D* **70**, <https://doi.org/10.1140/epjd/e2016-70428-6> (2016).

[70] T. Kovachy, S.-w. Chiow, and M. A. Kasevich, *Phys. Rev. A* **86**, 011606 (2012).

[71] J. C. Saywell, I. Kuprov, D. Goodwin, M. Carey, and T. Freegarde, *Phys. Rev. A* **98**, 023625 (2018).

[72] J. Saywell, M. Carey, M. Belal, I. Kuprov, and T. Freegarde, *J. Phys. B* **53**, 085006 (2020).

[73] J. Saywell, M. Carey, I. Kuprov, and T. Freegarde, *Phys. Rev. A* **101**, 063625 (2020).

[74] M. H. Goerz, M. A. Kasevich, and V. S. Malinovsky, in *Optical and Quantum Sensing and Precision Metrology*, Vol. 11700 (SPIE, 2021) p. 1170005.

[75] H. Ball, M. J. Biercuk, A. R. Carvalho, J. Chen, M. Hush, L. A. De Castro, L. Li, P. J. Liebermann, H. J. Slatyer, C. Edmunds, *et al.*, *Quantum Sci. Technol.* **6**, 044011 (2021).

[76] A. Bertoldi, C.-H. Feng, D. Naik, B. Canuel, P. Bouyer, and M. Prevedelli, *Phys. Rev. Lett.* **127**, 013202 (2021).

[77] R. Nourshargh, S. Lellouch, S. Hedges, M. Langlois, K. Bongs, and M. Holynski, *Comm. Phys.* **4**, 1 (2021).

[78] C. Deppner, W. Herr, M. Cornelius, P. Stromberger, T. Sternke, C. Grzeschik, A. Grote, J. Rudolph, S. Herrmann, M. Krutzik, A. Wenzlawski, R. Corgier, E. Chartron, D. Guéry-Odelin, N. Gaaloul, C. Lämmerzahl, A. Peters, P. Windpassinger, and E. M. Rasel, *Phys. Rev. Lett.* **127**, 100401 (2021).

[79] G. Feng, F. H. Cho, H. Katiyar, J. Li, D. Lu, J. Baugh, and R. Laflamme, *Phys. Rev. A* **98**, 052341 (2018).